CHAPTER 2

The Citric Acid-$Mn^{III,IV}O_2$(Birnessite) Reaction. Electron Transfer, Complex Formation, and Autocatalytic Feedback

2.1 Abstract

A synthetic MnO_2(birnessite) oxidizes citrate to 3-ketoglutarate and acetoacetate. Plots of citrate loss as a function of time, and plots of dissolved Mn^{II} and citrate oxidation product formation, all yield S-shaped curves, indicating autocatalysis. Increasing the citrate concentration decreases the induction period. The maximum rate (r_{max}) along the reaction coordinate follows a Langmuir-Hinshelwood dependence on citrate concentration. Increases in pH decrease r_{max} and increase the induction time. Adding Mn^{II}, Zn^{II}, orthophosphate, or pyrophosphate at the onset of reaction decreases r_{max}. Mn^{II} addition eliminates the induction period, while orthophosphate and pyrophosphate addition increase the induction period. Our findings indicate that two parallel processes are responsible. The first, relatively slow process involves the oxidation of free citrate by surface $Mn^{III,IV}$, yielding Mn^{II} and citrate oxidation products. The second process, which is subject to strong positive feedback, involves concerted reaction of Mn^{II} and citrate with surface $Mn^{III,IV}$, yielding citrate oxidation products and two equivalents of Mn^{II}.

2.2 Introduction

Citrate is a biological chelating agent that is released by the roots of all vascular plants *(1-5).* Whole-soil citrate concentrations as high as 50 μM have been reported *(1, 2).* In the rhizosphere, the zone of soil in direct contact with roots, citrate concentrations are believed to reach millimolar levels *(3).* Putative biogeochemical roles for citrate reflect its ability to chelate metal ions. In homogeneous solutions, citrate addition alleviates aluminum toxicity to biota by forming less toxic complexed species *(5-7).* In heterogeneous systems, ligand-assisted dissolution by citrate yields dissolved metal ion-citrate complexes. This is undesirable in the case of toxic metal ions, but beneficial in the case of nutrient metal ions like iron *(5, 8).* Ligand-assisted dissolution also solubilizes anionic mineral constituents. Hence, dissolution by citrate can release nutrient anions such as phosphate *(9-11).* Citrate is a component of many foods and pharmaceuticals *(12),* and is used in technological applications requiring an environmentally-benign chelating agent or dissolution agent, for example, for cleaning circuit boards *(13, 14).* Up to 400,000 tons of citrate and its derivatives are produced per year world-wide, with an annual 2-3 percent increase *(15).*

The overall abundance of manganese in the earth's crust is only one-fiftieth that of iron *(16).* $Mn^{III,IV}$ (hydr)oxides, like Fe^{III} (hydr)oxides, are much less soluble than (hydr)oxides comprised of the +II oxidation state. Mn^{II} diffusing out of reducing zones and into O_2-containing zones becomes oxidized, causing localized accumulation of Mn^{III}- and Mn^{IV}-containing (hydr)oxide solids *(17, 18).* Relative amounts of Mn^{III} and Mn^{IV} in such solids depend upon conditions present during their formation, and subsequent aging and chemical reaction. Natural samples invariably contain a mixture of the two oxidation

states. $Mn^{III,IV}$ (hydr)oxides are stronger oxidants than Fe^{III} (hydr)oxides, which explains their importance as oxidants of inorganic species *(19, 20)* and organic compounds *(21-27)*, including chelating agents *(24-27)*.

Citrate behavior in heterogeneous systems where adsorption *(28-31)* and ligand-assisted dissolution *(32, 33)* reactions are predominant have received the most attention. When a strong oxidant is present, e.g., $Mn^{III,IV}$ (hydr)oxides, the possibility that citrate serves as a reductant must also be considered. Godtfredsen and Stone *(34)* monitored the production of dissolved Mn (presumed to be Mn^{II}) during reaction of citrate with synthetic MnO_2(birnessite), and observed an induction period that decreased in duration as the citrate concentration was increased. Klewicki and Morgan *(26)* observed dissolved Mn^{III}, but no induction period, when a 20- to 30-fold excess of citrate was brought into contact with a (hydr)oxide preparation consisting primarily of Mn^{III}.

This study examines the reaction of citrate with a synthetic MnO_2(birnessite). Citrate oxidation products are identified, and the effects of pH and increasing citrate concentrations are explored. Additive effects (Mn^{II}, Zn^{II}, orthophosphate, and pyrophosphate) help us draw connections between solution speciation, surface speciation, and reaction rates. Dissolved Mn^{III} concentrations during reaction are quantified. S-shaped plots for citrate loss, Mn^{II} formation, and citrate oxidation-product formation as a function of time indicate that autocatalysis takes place. Our findings, supported by earlier observations *(26, 34)*, indicate that two parallel processes are responsible. The first, relatively slow process involves the oxidation of free citrate by surface $Mn^{III,IV}$, yielding Mn^{II} and citrate oxidation products. The second process, which is subject to

strong positive feedback, involves concerted reaction of Mn^{II} and citrate with surface $Mn^{III,IV}$, again yielding Mn^{II} and citrate oxidation products.

2.3 Materials and Methods

All solutions were prepared from reagent grade chemicals without further purification and distilled, deionized water (DDW) with a resistivity of 18 MΩ-cm (Millipore Corp., Milford, MA). Filter holders (Whatman Scientific, Maidstone, England) were soaked in 1 M ascorbic acid (Aldrich, Milwaukee, WI) and rinsed with distilled water and DDW. All bottles and glassware used to contain MnO_2(birnessite) suspensions were soaked in 1 M ascorbic acid, rinsed with distilled water, soaked in a 4 M nitric acid (J. T. Baker, Phillipsburg, NJ) bath overnight, rinsed with distilled water, and then rinsed with DDW water prior to use.

2.3.1 Chemicals. Citric acid, $ZnCl_2$, and NaCl were purchased from Aldrich. 3-Ketoglutaric acid was purchased from Lancaster Synthesis (Windham, NH). Lithium acetoacetate was purchased from Fluka (Buchs, Switzerland). NaH_2PO_4, Na_2HPO_4 and $MnCl_2 \cdot 4H_2O$ were purchased from J. T. Baker. Sodium butyrate (Aldrich), 2-morpholinoethansulfonic acid monohydrate (MES; Fluka, Buchs, Switzerland), and 3-[N-morpholino]propanesulfonic acid (MOPS; Sigma, St. Louis, MO) were used as pH buffers.

Our Mn^{III}-pyrophosphate stock solution contained a 20-fold excess of pyrophosphate. 13.4 mg $Mn^{III}(acetate)_3 \cdot 2H_2O$ (Aldrich) was dissolved in 50 mLs of a 20 mM disodium pyrophosphate (Fluka) solution that had been previously adjusted to pH 7 using NaOH (J. T. Baker) addition. After dissolution was complete, the pH was again

adjusted to pH 7. The solution was then filtered using a 0.1 µm pore size etch-tracked polycarbonate membrane (Whatman Scientific). Total dissolved Mn was determined in the filtered solution using flame atomic absorption spectrophotometry (AAS: Aanalyst 100, Perkin Elmer, Norwalk, CT). Following the method of Kostka et al. *(35)*, dissolved Mn^{III} was determined in this solution by UV-visible spectrophotometry (model UV-160U, Shimadzu Instrument Co., Kyoto, Japan) at a wavelength of 480 nm (molar absorptivity = 110 cm^{-1} M^{-1}). The Mn^{III}-pyrophosphate solution was stable enough to serve as a capillary electrophoresis (CE) standard for dissolved Mn^{III}. The solution was stored in a 4 ^{o}C refrigerator and remade every two weeks.

2.3.2 MnO_2 Synthesis and Characterization. MnO_2 herein refers to particles synthesized by precipitation of $Mn^{II}(OH)_2$(pyrochroite), followed by oxidation to $Mn^{III}OOH$(feitknechtite), and finally to $Mn^{III,IV}O_2$(birnessite) according to the method of Luo et al. *(36)*. A 750 mL solution of 5.0 M KOH (Aldrich) was placed in an ice bath, stirred vigorously, and sparged with Ar for 30 minutes to eliminate O_2. Slow addition of a sparged 600 mL solution of 0.5 mM $Mn^{II}(acetate)_2 \cdot 4H_2O$ (Aldrich) yielded a white suspension. Next, dropwise addition of 3000 mLs of a 4.4 M H_2O_2 (Aldrich) / 3.1 M KOH solution yielded a black suspension, along with bubbles and steam. Synthesis was complete when further addition of the H_2O_2 / KOH solution failed to generate bubbles and steam.

The synthesized particles were allowed to settle. The supernatant solution was removed and replaced with DDW. The particles were resuspended using sonication. This rinse procedure was repeated 5 times, in order to make the highly basic suspension less basic. 0.01 M HCl (J. T. Baker) was added dropwise to further decrease the pH to

approximately 7. At this point, the suspension pH was low enough for a centrifuge-based washing procedure. Centrifugation (RC5-B Sorvall/Kendro, Asheville, NC) at 7000 rpm for increasing periods of time (10 minutes to 6 hours) was performed. After 15 washing times, the specific conductivity of the supernatant solution was less than that of a 1×10^{-4} M KCl (Aldrich) solution. Dissolved manganese in the supernatant solution was less than the AAS detection limit (1.0 μM). The washed suspension was stored in a 4 ^{o}C refrigerator prior to use.

Particles from the original synthesized suspension were characterized by powder x-ray diffraction (XRD) and transmission electron microscopy (TEM). Freeze-dried particles (Lanconco Corp., Kansas City, MO) were also characterized and gave the same results as the particles from the original suspension. XRD yielded diffraction lines with the following d-spacings: 7.22, 3.59, 2.47, 2.36, 2.05, 1.74, and 1.42 Å. The d-spacings are consistent with the distorted hexagonal layered structure of MnO_2(birnessite) proposed by Manceau's group *(37).* The well-defined 7 Å basal d-spacing reflects the characteristic interlayer spacing of MnO_2(birnessite) *(37, 38).* TEM reveals that many of the MnO_2 sheets are curled. Curling of MnO_2(birnessite) sheets has been observed previously *(39),* and attributed to edge sections that are thicker than middle sections. The freeze-dried particles weigh 97.10 grams per mole of manganese. The BET multipoint N_2 adsorption method (Coulter 3100 BET Instrument, Miami, FL) was performed on a freeze-dried sample, and yielded a specific surface area of 174.3 m^2/g.

The average oxidation state of manganese was determined by iodometric titration *(40).* Prior to sampling, the MnO_2 suspension was rigorously stirred. The sample was reduced by an excess of KI (Fisher Chemical, Pittsburgh, PA) in 0.01 M HCl solution,

yielding a brown I_2 solution. Soluble starch indicator (Fisher Chemical) was then added, and the brown I_2 solution was back-titrated using $Na_2S_2O_3$. The endpoint was reached when the suspension was colorless. The average oxidation state was found to be +3.78. If we assume that Mn^{II} is not present, then this average oxidation state corresponds to 22 % Mn^{III} and 78 % Mn^{IV}.

2.3.3 Experimental Setup. *Degradation Experiments.* All batch experiments were conducted in 100 mL polypropylene bottles in a constant temperature circulating bath at 25 ± 0.2 ^{o}C and stirred with Teflon-coated stir bars. 10 mM butyrate ($5.0 \leq pH \leq 5.6$), MES ($6.0 \leq pH \leq 6.6$), or MOPS (pH 7.1) were employed to maintain constant pH. pH stability was verified by periodic measurement (Fisher Accumet 825MP meter with Orion Combination semi-micro probe; NIST-traceable standards). pH buffer concentrations were high enough to serve an additional purpose, maintenance of constant ionic strength conditions. No additional electrolyte was added.

Solutions containing organic substrate and pH buffer (plus additional constituents, as appropriate) were sparged with Ar (BOC gases, Baltimore, MD) for one hour prior to MnO_2 addition. Sparging was continued during the duration of the experiments. 4mL reaction suspension aliquots were collected at periodic intervals. Reactions were quenched by immediately filtering through 0.1 µm pore diameter track-etched polycarbonate filter membranes (Whatman). Filtered solutions were analyzed by AAS for total Mn and by capillary electrophoresis for additional species (see later section). Inorganic carbonate was not monitored because of possible losses arising from sparging.

Mn^{II} Adsorption Experiments. All experiments began by adding MnO_2 stock suspension, $MnCl_2$ solution, and DDW into 15 mL polypropylene bottles. Some

experiments employed HCl or NaOH addition to set the pH. In this instance, the ionic strength was low, near 0.04 mM. In other experiments, a 10 mM MOPS buffer (pH 7.1) was employed, yielding an ionic strength of approximately 5 mM. In a limited number of experiments, the ionic strength was raised by added 10 mM NaCl. A circulating constant temperature bath maintained the temperature at $25.0 \pm 0.2\ ^{o}C$. Stirring was performed using teflon-coated stir bars. Suspensions were equilibrated for four hours prior to filtration through 0.1 μm pore diameter track-etched polycarbonate filter membranes (Whatman). Filtered solutions were analyzed for total dissolved Mn using AAS.

2.3.4 Capillary Electrophoresis. A capillary electrophoresis unit from Beckman Coulter (P/ACE MDQ, Fullerton, CA) with diode-array UV-visible detector was used for all determinations. Detector bandwidth was set at 6 nm for 190 nm wavelength detection and 10 nm for all other wavelengths. Bare fused silica capillaries (Polymicro Technologies, Phoenix, AZ) with 75 μm ID × 60 cm total length were used for all separations. The effective length defined as the length from the inlet to the detector was 52 cm. Capillary and sample board temperature was thermostatted to $10\ ^{o}C$ during operation. Between separations, the capillary was sequentially rinsed by flushing DDW for 0.5 minute, 0.1 M NaOH for 1 minute, DDW again for 1 minute, and capillary electrolyte for 2 minutes. Sample injection employed 0.5 psi of positive pressure for 15 seconds. Anion mode with constant applied voltage (-22 kV) was employed for all separations.

In previous efforts to obtain metal ion and chelating agent speciation information *(41)* a non-complexing CE electrolyte such as 50 mM MOPS (pH 7.0) and 0.5 mM TTAB was employed. Using this CE electrolyte with Mn^{III}-pyrophosphate solutions,

however, yielded a baseline increase and a broad, unusable peak. When Mn^{II}-containing stock solutions were injected, no peak was obtained. Measured currents declined with successive injections, which we conclude was caused by formation of inorganic precipitates, leading to column clogging. The unusable or undetectable peaks are likely caused by ligand exchange during electromigration, which is reasonable based upon the fact that Mn^{III} is more substitution-labile than other +III metal ions and Mn^{II} is more substitution-labile than other +II metal ions that we have worked with in the past *(41, 42)*. Since the CE electrolyte does not contain ligands capable of solubilizing Mn^{III}, any electric field-induced dissociation will lead to Mn^{III} precipitation within the column. Precipitation of Mn^{II} within the column is harder to explain, but may involve precipitation with inorganic carbonate, inadvertently added to the CE electrolyte through contact with air.

We elected to use a CE electrolyte consisting of 20 mM pyrophosphate, 0.4 mM TTAB, and 2 mM orthophosphate (pH 9.5) for our CE determinations. Pyrophosphate is a strong enough chelating agent for Mn^{III} and present in a high enough concentration to capture all the Mn^{III} in our samples during electromigration. A sharp, symmetrical peak, easily discernable at a detection wavelength of 235 nm, provided the means of measuring $Mn^{III}(aq)$ (total dissolved Mn^{III}). logK values for Mn^{II} complexes with pyrophosphate are significantly lower than those for Mn^{III} *(43, 44)*. The sharpest, most symmetrical peak for Mn^{II} is obtained when a CE electrolyte with a pH of 9.5 is employed. Lowering the pH of the CE electrolyte causes more and more peak broadening and tailing, and an increase in the baseline. The $Mn^{II}(aq)$ peak is more discernable at 214 nm than at 235 nm, consistent with its known spectral qualities *(43)*. Although no attempt was made to

quantify Mn^{II} using CE, the pyrophosphate-TTAB-orthophosphate CE electrolyte did succeed in preventing measured current decline and increasing column life, especially at pH 9.5.

Citrate and its oxidation products only absorb light at wavelengths less than 210 nm. Pyrophosphate does not adsorb light in this region. Indeed, the pyrophosphate-TTAB-orthophosphate CE electrolyte allowed simultaneous determination of Mn^{III}(aq), un-reacted citrate, and citrate oxidation products.

2.4 Results and Discussion

2.4.1 Mn^{II} Adsorption onto MnO_2. In suspensions containing 20 μM $MnCl_2$ and 200 μM MnO_2, the extent of Mn^{II} adsorption increased from nearly negligible levels at pH values below 5.7 to nearly 100 % for pH values above 7.7 (Figure 2.1a). Adding 10 mM NaCl did not perceptibly affect the extent of adsorption.

Adsorption as a function of total added Mn^{II} ($TOTMn^{II}$) at fixed MnO_2 loading (200 μM) (Figure 2.1b) was investigated at a fixed pH of 7.1 using a 10 mM MOPS buffer. The data were fitted using a Langmuir Adsorption Isotherm:

$$[Mn^{II}(ads)] = \frac{[Mn^{II}(ads, max)]K[Mn^{II}(aq)]}{1 + K[Mn^{II}(aq)]}$$

$[Mn^{II}(ads,max)]$ (9.4 μM), which corresponds to the maximum extent of adsorption, and the adsorption constant K (9.0×10^5 M^{-1}) were obtained using the Marquardt-Levenberg Algorithm *(45)*.

2.4.2 Citrate Oxidation Products. Filtered reaction solutions from citrate-containing MnO_2 suspensions yielded new CE peaks at 2.50, 2.58, 2.64, 2.89, and 3.58

minutes, regardless of the reaction conditions employed. The first, second and fifth peaks are assigned to citrate, 3-ketoglutarate and acetoacetate, respectively, based on peak growth following injection of authentic samples. Similarly, the third and fourth peaks are assigned to Mn^{III}(aq) and Mn^{II}(aq), respectively, based upon peak growth following injection of Mn^{III}-pyrophosphate and Mn^{II} standard solutions.

Carboxylate and carbonyl groups only absorb light in the far UV, and hence it is reasonable that a low wavelength (190 nm) provided the best quantifications of organic analytes. Citrate and 3-ketoglutarate, each possessing three C=O chromophoric groups, yield detection limits of 2 μM. Acetoacetate, with two such groups, has a slightly higher detection limit (5 μM). Molecules with a greater charge yield a shorter electromigration time, i.e., citrate (-3) < 3-ketoglutarate (-2) < acetoacetate (-1).

In previous experiments performed in homogeneous solutions, 3-ketoglutarate has been identified as a product of citrate oxidation by Mn^{II} plus O_2 *(46)*, by Cr^{VI} *(47)*, and by HOCl *(48)*. Photolysis of Fe^{III}-citrate complexes also yields 3-ketoglutarate *(49)*. Acetoacetate is mentioned as a second product in some of these studies *(48, 49)*.

The oxidative decarboxylation reaction responsible for the conversion of citrate into 3-ketoglutarate *(48)* is shown in Figure 2.2a. It is well established that carboxylates with both an α-hydroxyl group and an α-hydrogen atom undergo two-electron oxidation to corresponding aldehydes or ketones *(49, 50)*. Citrate does not possess the α-hydrogen group, but CO_2 exit accompanying electron abstraction and hydrogen bonding within the 3-ketoglutarate product facilitate the oxidation reaction *(48)*.

As shown in Figure 2.2b, 3-ketoglutarate is converted into acetoacetate by a non-redox decarboxylation rearrangement reaction *(51)*. The electron-withdrawing property

of the β-carbonyl group is responsible; it serves as an "electron sink" for the two electrons constituting the C-C bond undergoing cleavage. Hydrogen-bonding and the formation of a 6-membered ring transition state are believed responsible for the observed acid catalysis exhibited by this reaction *(51)*. Divalent metal ions including Mn^{2+}(aq) catalyze decarboxylation *(51)*. The reaction is driven by the stabilized enol tautomer via formation of a 6-membered ring metal chelate *(51)*.

2.4.3 Illustrative Time Course Plot – Autocatalysis. MnO_2 suspensions, at pH 7.1 in the absence of citrate, yielded dissolved Mn concentrations that were slightly above the detection limit (1.0 μM), but only after three days. Citrate loss was not observed in MnO_2-free solutions, regardless of pH.

Figure 2.3 presents an illustrative time course plot for reaction of 200 μM citrate with 200 μM MnO_2 at pH 7.1. Citrate loss, total dissolved manganese (Mn(aq)) production, and 3-ketoglutarate production all yield S-shaped curves. CE peaks corresponding to acetoacetate are only discernable after 16 hours of reaction. At the last sampling point, [acetoacetate] is only 6 % of [3-ketoglutarate]. The sum [citrate] + [3-ketoglutarate] + [acetoacetate] remains constant as the reaction progresses, indicating that mass balance is obeyed.

Total dissolved manganese (Mn(aq)) determined by AAS is comparable to [3-ketoglutarate] before the inflection point in the S-shaped curves, but slightly higher afterwards. Dissolved Mn^{III} (Mn^{III}(aq)) determined using CE rise and then fall. At its highest point, Mn^{III}(aq) is only 4 % of Mn(aq). Hence, total dissolved manganese is primarily Mn^{II}. The time course plot for Mn^{III}(aq) should be interpreted with caution, however, since all the data points are within a factor of 3 of the detection limit (about 1.5

μM). It is interesting to note that the maximum in Mn^{III}(aq) lies close to the inflection points of the three S-shaped curves.

Three reaction stages are marked in Figure 2.3, which are useful in making run-to-run comparisons. Stage 1 corresponds to the induction period seen in the S-shaped curve. Stage 2 corresponds to a time interval bracketing the inflection point, where the highest rate of change is observed. Stage 3 is the final change, during which a significant decline in reaction rate is observed.

The predominance of Mn^{II}(aq) over Mn^{III}(aq) and the appearance of citrate oxidation products are reminiscent of reductive dissolution reactions *(52)*. The simplest representation of a reductive dissolution reaction involves surface sites (S) reacting with reductant (A) to yield reduced metal ions (C) and oxidation products (P):

$$A + S \longrightarrow C + P \qquad k_1 \tag{1}$$

This reaction is not, however, sufficient to explain Godtfredsen and Stone's *(34)* observation of an induction period in Mn(aq). At minimum, two reactions in series are required. (One possible scheme involves exponential decay of reactant A followed by increases in the concentrations of one or more intermediates. After a time delay set by the magnitude of a second (or third) rate constant, final products appear.)

The S-shaped curve with induction period appearance of the time course plot for citrate is important, because it cannot be explained by simple reactions in series. Positive feedback, i.e., acceleration of the forward reaction by at least one reaction product, must be invoked. We retain Reaction 1, but add a second reaction in parallel:

$$A + S + C \longrightarrow 2C + P \qquad k_2 \tag{2}$$

Reactions 1 and 2 constitute a complete autocatalysis scheme. Reaction 1 generates C to initiate Reaction 2, and Reaction 2 introduces positive feedback *(53, 54)*. Autocatalytic reactions of this kind have been extensively investigated in solution *(54, 55)*, but relatively little is known about heterogeneous autocatalytic reactions *(56)*. It is necessary to account for changes in surface site concentration. Our experimental system probably lies somewhere between the following two cases: (i) All surface sites are accessible at the onset of reaction. The "concentration" of sites decreases in proportion to the amount of dissolution that has taken place, i.e., $[S] = [S]_o - [P]$. (ii) The fraction of surface sites accessible at the onset of the reaction is low, and consumption of an accessible site exposes a new accessible site. Hence, the concentration of sites remains the same, i.e., $[S] = [S]_0$.

We will employ Case (ii), the mathematically simplest. Since the concentration of accessible surface sites is considered constant, we can write $k_1^* = k_1[S]_0$ and $k_2^* = k_2[S]_0$. Rate r, corresponding to production of organic oxidation products P, is the sum of the rates of Reactions 1 and 2:

$$r = \frac{d[P]}{dt} = r_1 + r_2 = k_1^*[A] + k_2^*[A][C] \qquad (3)$$

Setting $x = ([A]_0 - [A]) = [P] = [C]$ yields:

$$\frac{dx}{dt} = k_1^*([A]_0 - x) + k_2^*([A]_0 - x)x \qquad (4)$$

Integration yields:

$$\ln\left(\frac{(k_1^* + k_2^*x)[A]_0}{k_1^*([A]_0 - x)}\right) = (k_1^* + k_2^*[A]_0)t \qquad (5)$$

To serve as illustration, values of k_1* and k_2* have been selected for goodness-of-fit to an experiment (not shown) performed under the following conditions: 50 μM citrate, 200 μM MnO_2, and 10 mM MOPS buffer (pH 7.1). Figure 2.4a represents our best fit to Equation 4; the upper plot shows the simulated time course plot, and the lower plot shows r_1, r_2, and r as a function of time.

The highest value of r_1 is found at the onset of reaction, where x = 0. It decreases over time owing to decreases in [A]. Setting dr_2/dx equal to zero and solving the resulting equation tells us that the maximum value of r_2 is achieved when $x = [P] = [C] = (1/2)[A]_o$. This conclusion makes sense since r_2 is proportional to the product [A][C]. Reaction progress accelerates reaction by yielding C, but decelerates reaction by decreasing [A]; the highest rate corresponds to the midpoint.

To explore how the value of k_1^* affects time course plots, its value is decreased by a factor of ten in Figure 2.4b, and increased by a factor of ten in Figure 2.4c. In a similar manner, Figures 4d and 4e explore the effect of lowering and raising k_2^*. Inspection of the x-axis scales needed to display the entire time course is informative. A decrease in either k_1^* or k_2^* increases the time required to reach a particular reaction progress goal. The ratio k_1^*/k_2^* is also very informative. No induction period is observed when the ratio is high, and a low value of the ratio insures that an induction period will exist.

For practical reasons, we will take a different approach towards making quantitative run-to-run comparisons. Rates corresponding to the Stage 2 portion of each run (r_{max}, in units of μM/h) will be obtained from slopes of [3-ketoglutarate] versus time plots (Figure 2.3). Four or more points in the vicinity of the inflection point defining a straight line (as indicated by an r^2 value greater than 0.99) will be used to calculate this

slope. No attempt will be made to quantify the duration of Stage 1, which corresponds to the induction period, but trends in increasing or decreasing induction period will be pointed out. Whenever an induction period is observed, we can conclude, based upon our model, that Reaction 2 is the predominant contributor to the measured value of r_{max}.

2.4.4 Reaction Stoichiometry. The identification of 3-ketoglutarate and acetoacetate as the sole oxidation products of citrate provides an opportunity to check the redox stoichiometry of the reaction. We will represent citrate as $R_2C(OH)COO^-$ and 3-ketoglutarate as RC(O)R. Note that the conversion of 3-ketoglutarate into acetoacetate is not a redox reaction, and hence the sum of their concentrations is the true reflection of reaction progress. A pure Mn^{IV} (hydr)oxide (represented by $Mn^{IV}O_2(s)$) would yield one mole of Mn^{II} per mole of citrate oxidized:

$$R_2C(OH)COO^- + Mn^{IV}O_2(s) + 2H^+ = RC(O)R + HCO_3^- + Mn^{2+} + H_2O \qquad (6)$$

A pure Mn^{III} (hydr)oxide (represented by $Mn^{III}OOH(s)$) would yield two moles of Mn^{II} per mole of citrate oxidized:

$$R_2C(OH)COO^- + 2Mn^{III}OOH(s) + 4H^+ = RC(O)R + HCO_3^- + 2Mn^{2+} + 3H_2O \qquad (7)$$

As noted earlier, the average oxidation state of the MnO_2 preparation used in our experiments was 3.78. Representing this reaction as $Mn(OH)_{3.78}(s)$ leads to the following redox stoichiometry:

$$R_2C(OH)COO^- + 1.12Mn(OH)_{3.78}(s) + 2.25H^+ = RC(O)R + HCO_3^- + 1.12Mn^{2+} + 3.24H_2O \qquad (8)$$

Hence, the (hydr)oxide employed in our experiments should yield 1.12 moles of Mn^{II} per mole of citrate oxidized.

The yield of Mn^{II} per mole of citrate oxidized, which we can call n, requires that dissolved plus adsorbed concentrations of the three products be known:

$$n = \frac{TOTMn^{II}}{[TOT\ 3\text{-ketoglutarate}] + [TOT\ acetoacetate]} \quad (9)$$

Total concentrations are not experimentally measurable quantities. We can, however, calculate an "apparent" yield n', using dissolved concentration measurements:

$$n' = \frac{[Mn^{II}(aq)]}{[3\text{-ketoglutarate(aq)}] + [acetoacetate(aq)]} \quad (10)$$

At the MnO_2 loadings employed here, adsorption of 3-ketoglutarate and acetoacetate is believed to be negligibly low, while adsorption of Mn^{II} is expected to be significant. For this reason, n' should be less than or equal to n.

Figure 2.5 shows values of n' as a function of time for the experiment presented in Figure 2.3. Values of n' rise from 0.93 to 1.19 during the first 5 hours of reaction. The eight data points collected between 5 and 21 hours of the reaction yield a mean value of 1.20 for n' with a 95 % confidence interval of ±0.08. The expected value for n (1.12) falls within this confidence interval.

Initially low values of n' can arise from either Mn^{II} retention by the MnO_2 surface and/or preferential reaction of Mn^{IV} in comparison to Mn^{III}. Both postulated phenomena should diminish in importance as the reaction progresses. Mn^{II} retention should diminish because more and more Mn^{II} must compete for fewer and fewer adsorption sites. Preferential consumption of Mn^{IV} will eventually deplete the surface and shift reaction towards Mn^{III}.

2.4.5 Effect of Zn^{II} and Mn^{II} Addition. Adding 200 μM $Zn^{II}Cl_2$ in the absence of citrate results in the release of a small amount of dissolved Mn (approximately 2.5

μM), presumably through a cation exchange mechanism. Adding 10 μM $Zn^{II}Cl_2$ at the onset of reaction of 200 μM citrate with 200 μM MnO_2 at pH 7.1 (Figure 2.6a) yields a slight increase in 3-ketoglutarate production during Stage 1, and a slight decrease in production during Stage 3. The induction period is slightly shortened, and r_{max} decreases by 13 % (Table 2.1). Adding 200 μM $Zn^{II}Cl_2$ effectively shuts off 3-ketoglutarate production.

As shown in Figure 2.6b, 10, 200, 500, and 1000 μM added $Mn^{II}Cl_2$ all eliminate the induction period. It is interesting to note that r_{max} obtained when 10 μM $Mn^{II}Cl_2$ is added is the same as the value obtained when no $Mn^{II}Cl_2$ is added (Table 2.1). Increasing the added $Mn^{II}Cl_2$ concentration 100-fold causes only a 3.4-fold decrease in r_{max}.

Reactions 1 and 2 presented earlier are simplistic in that they do not explicitly account for adsorption (either inner sphere or outer sphere), which is a prerequisite for electron transfer. To provide the basis for evaluating metal ion addition effects, the following mass balance equations are informative:

$$Mn^{II}_T = [Mn^{II}(aq)] + [Mn^{II}\text{-Citrate}(aq)] + [S\text{-}Mn^{II}] + \underline{[(S, Mn^{II}, Citrate)]} \quad (11)$$

$$Zn^{II}_T = [Zn^{II}(aq)] + [Zn^{II}\text{-Citrate}(aq)] + [S\text{-}Zn^{II}] + \underline{[(S, Zn^{II}, Citrate)]} \quad (12)$$

$$Citrate_T = [Citrate(free, aq)] + [Mn^{II}\text{-Citrate}(aq)] + [Zn^{II}\text{-Citrate}(aq)] + \underline{[S\text{-Citrate}]} + \underline{[(S, Mn^{II}, Citrate)]} + \underline{[(S, Zn^{II}, Citrate)]} \quad (13)$$

$$S_T = [S(free)] + [S\text{-}Mn^{II}] + [S\text{-}Zn^{II}] + \underline{[S\text{-Citrate}]} + \underline{[(S, Mn^{II}, Citrate)]} + \underline{[(S, Zn^{II}, Citrate)]} \quad (14)$$

$Mn^{III,IV}$ surface sites are denoted as "S". For each component, both dissolved and adsorbed species are included in the mass balance. No attempt is made to denote protonation level or bonding arrangement. (S, Zn^{II}, Citrate) and (S, Mn^{II}, Citrate) denote

surface ternary complexes that may be inner-sphere, ligand-like complexes where citrate serves as a bridge, inner-sphere, metal-like complexes where Zn^{II} or Mn^{II} serve as a bridge, or outer sphere complexes where Zn^{II}Citrate or Mn^{II}Citrate complexes are associated with surface sites, yet maintain their hydration shells. 3-Ketoglutarate and acetoacetate production can potentially arise from any of the underlined species.

When redox-inert Zn^{II} is added, [Zn^{II}-Citrate(aq)], [S-Zn^{II}], and [(S, Zn^{II}, Citrate)] increase at the expense of citrate species and surface site species that do not contain Zn^{II}. Table 2.2 presents equilibrium calculations for MnO_2-free solutions, based upon logK values available in the literature *(57)*. 10 μM Zn^{II} has only a slight effect on [Mn^{II}-Citrate(aq)], while 200 μM Zn^{II} causes a 42 % decrease in [Mn^{II}-Citrate(aq)]. The surface species S-Zn^{II} is redox inert. If we assume that all surface species denoted as (S, Zn^{II}, Citrate) are either redox-inert or present at insignificantly low concentrations, the inhibitory effects arising from Zn^{II} addition are easily explained.

What can we say about Mn^{II} speciation with respect to the $Mn^{II}Cl_2$ addition experiments? Langmuir adsorption constants derived from Figure 2.1 indicate that 73 % of Mn^{II} is adsorbed in citrate-free suspensions containing 10 μM Mn^{II} and 200 μM MnO_2 at pH 7.1. Equilibrium calculations presented in Table 2.2 indicate that 85 % of Mn^{II} is complexed in MnO_2-free solutions containing 10 μM Mn^{II} and 200 μM citrate at pH 7.1. If for the moment we ignore citrate adsorption, then a Langmuir-type description of adsorption and the Mn^{II}-citrate solution speciation model can be combined into a simple "complete system" equilibrium model. Calculations indicate that for suspensions containing 10 μM Mn^{II}, 200 μM citrate, and 200 μM MnO_2, 40 % of the Mn^{II} is adsorbed and 51 % is coordinated to citrate in solution.

2.4.6 Effect of Citrate Concentration. As shown in Figure 2.7a, citrate concentrations ranging from 50 μM to 5.0 mM at pH 7.1 all yield S-shaped curves. The 100-fold increase in citrate concentration shortens the induction period from approximately 10 hours to 40 minutes. A slight increase in the Stage 1 reaction rate is discernible from changes in the initial slope, but the 3-ketoglutarate concentrations during this stage are too low to provide quantitative estimates of rate. Changes in r_{max}, the highest rate of reaction within the Stage 2 portion of the time course plot, are readily quantified. The 100-fold increase in citrate concentration yields a 25-fold increase in r_{max}, and saturation kinetics are apparent (Figure 2.7b).

According to Reactions 1 and 2, raising $[citrate]_0$ increases both r_1 and r_2, which decreases the induction period and increases the overall rate r. Since an induction period is observed at all five citrate concentrations, we can conclude that r_2 is the predominant contributor to r_{max}. Although we cannot yet identify the species responsible for autocatalysis, a Langmuir-Hinshelwood rate expression *(58, 59)* can provide information about its relative abundance:

$$r_{max} = \frac{r_{max,\,sat} K[citrate]_0}{1 + K[citrate]_0} \qquad (15)$$

$[citrate]_0$ represents initial the citrate concentration, $r_{max,\,sat}$ represents the value r_{max} when saturation of the surface with citrate has been achieved, and K represents the citrate adsorption constant. The parameters $r_{max,sat}$ = 85 μM/h and $K = 7.2 \times 10^2\ M^{-1}$ were obtained from the data in Figure 2.6b using the same nonlinear least squares method employed earlier with the Langmuir Adsorption Isotherm. Most of our experiments employed 200 μM citrate, 200 μM MnO_2, and 10 mM MOPS buffer (pH 7.1). Under

these conditions, $r_{max}/r_{max,sat}$ is equal to 0.16, indicating that the species responsible for autocatalysis is present at 16 % of its maximum value.

2.4.7 Effect of Orthophosphate and Pyrophosphate Addition. As shown in Figure 2.8, 5.0 mM orthophosphate and 0.2 mM pyrophosphate approximately doubled the induction period and decreased r_{max} by half.

Lewis Base additives may interfere with the reaction by (i) adsorbing onto $Mn^{III,IV}$ surface sites and (ii) forming complexes with Mn^{II} in solution. The first possibility is quite real yet difficult to evaluate since, for both Lewis Bases, loss from solution is not high enough to detect under the reaction conditions considered (200 μM MnO_2, pH 7.1). The second possibility can be evaluated by performing equilibrium calculations which employ complex formation constants reported in the literature *(57)*, as we have done in Table 2.2. The two additive concentrations employed (5.0 mM orthophosphate, and 0.2 mM pyrophosphate) decrease $\Sigma[Mn^{II}H_x(citrate)]$ in roughly comparable amounts (32 % and 27 %, respectively.)

In Figure 2.9, results from three addition experiments are compared with results from an additive-free experiment. Adding Mn^{II} alone or Mn^{II} plus pyrophosphate eliminates the induction period entirely. Adding pyrophosphate alone causes the induction period to increase. Pyrophosphate-only and Mn^{II} plus pyrophosphate experiments yielded similar r_{max} values (7.0 and 6.1 μM/h, respectively) that are two-times lower than r_{max} values measured in additive-free and Mn^{II}-only experiments.

As far as the induction period is concerned, Mn^{II} and pyrophosphate additives work at cross-purposes, with Mn^{II} exerting the slightly stronger effect at the concentrations employed. Adding Mn^{II} allows Reaction 2 to predominate throughout the

entire time course; there is no need to wait for Reaction 1 to generate enough Mn^{II} to form the autocatalytic reagent. The lowering effect of pyrophosphate on r_{max} is especially noteworthy, since it is observed whether or not Mn^{II} is added. The effect of orthophosphate on the autocatalytic mechanism appears similar to that of pyrophosphate, but much weaker.

2.4.8 Effect of pH. S-shaped time course plots are obtained throughout the range $5.1 < pH < 7.1$ (Figure 2.10). Decreasing the pH from 7.1 to 6.0 causes the induction period to decrease from approx. 2 hours to approximately 15 minutes. Further decreasing the pH to 5.1 does not significantly alter the duration of the induction period. Decreasing the pH from 7.1 to 5.1 causes an 8-fold increase in r_{max} (Figure 2.10b). Connecting successive pairs of points in a log-log plot (Figure 2.10b) yields an apparent order with respect to $[H^+]$ that is nearly zeroth-order between pH 5.1 and 5.6, but becomes more sensitive to $[H^+]$ as the pH is increased.

For a MnO_2-free solution containing 10 μM Mn^{II} and 200 μM citrate, an equilibrium calculation performed for pH 5.1 in the manner of Table 2.2 yields 2.72 μM $Mn^{II}cit^-$, 6.67 μM Mn^{2+}, and 0.61 μM $Mn^{II}Hcit^0$. The sum of the concentrations of all Mn^{II}-citrate complexes is therefore 2.5-times lower at pH 5.1 than at 7.1. Figure 2.1 indicates that the amount of Mn^{II} adsorbed in citrate-free MnO_2 suspensions at pH 5.1 is substantially less than at pH 7.1.

What do we know about citrate adsorption as a function of pH? Anion adsorption onto MnO_2(birnessite), a cation-exchange phase with a low pH_{zpc}, is low, and not well understood *(60).* If adsorption onto conventional (hydr)oxide phases such as FeOOH(s, goethite) *(30)* or AlOOH(s, pseudoboehmite) *(61)* in an appropriate analogy, then a

substantial increase in adsorption with decreasing pH is expected *(62)*. Unlike dissolved Mn^{II}-citrate complexes and unlike adsorbed Mn^{II}, expected trends in adsorbed citrate as a function of pH actually follow the same trend as the rate data shown in Figure 2.10.

2.4.9 The Autocatalytic Step. Redox reactions involving (hydr)oxide surfaces are notoriously complex. Our experimental findings are sufficient, however, to clarify some details regarding the molecular-level mechanism of the citrate-MnO_2 reaction.

Equilibrium constants for Mn^{III}-citrate complexes are not available in the literature. Observed Mn^{III}(aq) concentrations as high as 4.8 μM (Figure 2.3) point to the existence of such complexes, since aquo and hydroxo Mn^{III} species are sparingly soluble with respect to $Mn^{III}OOH$(see Supporting Information) and since 3-ketoglutarate and acetylacetate are considerably weaker chelating agents than citrate. An appraisal of Mn^{III}-citrate complexes based on analogies with the Fe^{III} system (see Supporting Information) suggests that $Mn^{III}(OH)CIT^{-}$ is the predominant dissolved Mn^{III} species under the conditions employed in our experiments. Using the Mn^{III}(aq) measurements reported in Figure 2.3, a lower estimate of $K = 10^{14.67}$ for the reaction $Mn^{3+} + citrate^{3-} + H_2O = Mn^{III}(OH)(citrate)^{-} + H^{+}$ is obtained (see Supporting Information).

Dissolved Mn^{III}-citrate complexes may arise from (i) ligand-assisted dissolution of the 22 % of manganese atoms within the MnO_2 preparation that was originally in the +III oxidation state; (ii) ligand-assisted dissolution of Mn^{IV} atoms that have been reduced to Mn^{III} and (iii) oxidation of Mn^{II}-citrate complexes by the remaining MnO_2 reactant. Mechanism i has been previously confirmed by Klewicki and Morgan *(26)* in their study of the citric acid-assisted dissolution of a MnOOH(feithnecktite)/Mn_3O_4(hausmannite)

mixture. In order to evaluate Mechanism iii, three half reactions from the Supporting Information are pertinent:

$Mn^{IV}O_2(s) + 3H^+ + 2e^- = Mn^{2+} + 2H_2O \quad E^o = 1.29 \text{ volts} \quad E = 1.00 \text{ volts} \quad (16)$

$Mn^{III}OOH(s) + 3H^+ + e^- = Mn^{2+} + 2H_2O \quad E^o = 1.50 \text{ volts} \quad E = 0.834 \text{ volts} \quad (17)$

$Mn^{III}(OH)(citrate)^- + H^+ + e^- = Mn^{II}(citrate)^- + H_2O$

$E^o = 1.00 \text{ volts} \quad E = 0.568 \text{ volts} \quad (18)$

E^o for Reactions 16 and 17 are obtained from the literature, while E^o for Reaction 18 is an estimate. To calculate E values relevant to Figure 2.3, we employed 1.51×10^{-6} M Mn^{2+}, 8.46×10^{-6} M $Mn^{II}(citrate)^-$, 4.6×10^{-6} M $Mn^{III}(OH)(citrate)^-$, and pH 7.1 (based upon calculations in Table 2.2 and in Supporting Information.) A comparison of reduction potentials indicates that surface-bound $Mn^{III/IV}$ is thermodynamically capable of oxidizing $Mn^{II}(citrate)^-$ to $Mn^{III}(OH)(citrate)^-$. Mechanistically, the metal-to-metal electron transfer could occur via a ligand-like, inner-sphere ternary precursor complex, metal-like, inner-sphere ternary precursor complex, or outer-sphere precursor complex. Irrespective of the nature of the precursor complex, metal-to-metal electron transfer is likely to be fast.

Oxidation of $Co^{II}(EDTA)^-$ *(63)* and a variety of Cr^{III}-aminocarboxylate complexes *(64)* by manganese(III,IV) (hydr)oxides has been reported. Although there are no prior reports of interfacial manganese-to-manganese electron transfer, analogous iron-to-iron reactions have been extensively investigated. Fe^{II}-chelating agent complexes and their subsequent reaction with surface-bound Fe^{III} are key aspects of the dissolution of Fe_3O_4(magnetite) by oxalate *(65, 66)*, Fe_2O_3(hematite) by ascorbate/EDTA *(67)*, and Fe_2O_3(hematite) by ascorbate/oxalate *(67)*. Similar mechanisms are operative in the

dissolution of FeOOH(goethite) by oxalate/Fe^{II} *(68)*, EDTA/Fe^{II} *(69)*, malonate/Fe^{II} *(70)* and citrate/Fe^{II} *(70)*.

$Mn^{III}(OH)(citrate)^-$ decomposes by intramolecular electron transfer. A half life in the range of 4 to 10 hours was reported by Klewicki and Morgan *(71)* for a solution consisting of 0.30 mM Mn^{III}-citrate, 0.20 mM Mn^{II}-citrate, and 25 mM total dissolved citrate at pH 7.4. Extrapolation to a new set of conditions can not be made. In both Klewicki and Morgan's experiments and our own, bimolecular reactions between $Mn^{III}(OH)(citrate)^-$ and free citrate ions cannot be ruled out. When $Mn^{III,IV}$ (hydr)oxides are present, as in our experiments, it is also conceivable that $Mn^{III,IV}$ surface sites somehow catalyze the decomposition of $Mn^{III}(OH)(citrate)^-$.

Source and sink terms for Mn^{III}-citrate, and a generalized scheme for Reaction 2, the autocatalytic step, are shown in Figure 2.11. This $Mn^{III/II}$ citrate autocatalytic cycle is the first of its kind proposed for a manganese-based redox system. Previously investigated organic reductants *(23, 72)* did not yield autocatalysis because, unlike citrate, they were unable to form appreciable concentrations of dissolved Mn^{II} and Mn^{III} complexes. Intramolecular electron transfer within Mn^{III}-citrate complexes, which releases Mn^{II} to repeat the cycle, is also essential for autocatalysis.

Acknowledgements—This work was supported by Grant NumberR-82935601 from the U.S. Environmental Protection Agency's Science to Achieve Results (STAR) program. Although the research described in this article has been funded wholly by this grant, it has not been subject to EPA review and therefore does not necessarily reflect the views of the Agency, and no official endorsement should be inferred. We thank Dr. Anne-

Claire Gaillot (Department of Earth & Planetary Sciences, Johns Hopkins University) for her help with MnO_2(birnessite) characterization. We thank Dr. Roland Glantz and Wei Long (Department of Geography & Environmental Engineering, Johns Hopkins University) for their help with MATLAB programming. We also thank Prof. James J. Morgan for thoughtful discussion and insightful comments.

2.5 Literature Cited

(1) Strobel, B. W. Influence of vegetation on low-molecular-weight carboxylic acids in soil solution - a review. *Geoderma* **2001**, 99, 169-198.

(2) Strobel, B. W., Bernhoft, I., and Borggaard, O. K. Low-molecular-weight aliphatic carboxylic acids in soil solutions under different vegetations determined by capillary zone electrophoresis. *Plant Soil* **1999**, 212, 115-121.

(3) Jones, D. L. Organic acids in the rhizosphere - a critical review. *Plant Soil* **1998**, 205, 25-44.

(4) Dinkelaker, B., Romheld, V., and Marschner, H. Citric-acid excretion and precipitation of calcium citrate in the rhizosphere of white lupin (lupinus-albus l). *Plant Cell Environ.* **1989**, 12, 285-292.

(5) Gerke, J., Romer, W., and Jungk, A. The excretion of citric and malic-acid by proteoid roots of lupinus-albus l - effects on soil solution concentrations of phosphate, iron, and aluminum in the proteoid rhizosphere in samples of an oxisol and a luvisol. *Zeitschrift Fur Pflanzenernahrung Und Bodenkunde* **1994**, 157, 289-294.

(6) Jones, D. L. and Kochian, L. V. Aluminium-organic acid interactions in acid soils. 1. Effect of root-derived organic acids on the kinetics of al dissolution. *Plant Soil* **1996**, 182, 221-228.

(7) Fransson, A. M., Vinogradoff, S., Godbold, D. L., van Hees, P. A. W., and Jones, D. L. Aluminum complexation suppresses citrate uptake by acid forest soil microorganisms. *Soil Biol. Biochem.* **2004**, 36, 353-357.

(8) Furrer, G. and Stumm, W. The coordination chemistry of weathering. 1. Dissolution kinetics of δ-Al_2O_3 and BeO. *Geochim. Cosmochim. Acta* **1986**, 50, 1847-1860.

(9) Veneklaas, E. J., Stevens, J., Cawthray, G. R., Turner, S., Grigg, A. M., and Lambers, H. Chickpea and white lupin rhizosphere carboxylates vary with soil properties and enhance phosphorus uptake. *Plant Soil* **2003**, 248, 187-197.

(10) Ae, N., Arihara, J., Okada, K., Yoshihara, T., and Johansen, C. Phosphorus uptake by pigeon pea and its role in cropping systems of the Indian subcontinent. *Science* **1990**, 248, 477-480.

(11) Geelhoed, J. S., Van Riemsdijk, W. H., and Findenegg, G. R. Simulation of the effect of citrate exudation from roots on the plant availability of phosphate adsorbed on goethite. *Eur. J. Soil Sci.* **1999**, 50, 379-390.

(12) Kirk, R. E. and Othmer, D. F. *Kirk-Othmer Encyclopedia of Chemical Technology*. 2004, New York: John Wiley.

(13) Rehim, S. S. A., Sayyah, S. M., and El Deeb, M. M. Corrosion of tin in citric acid solution and the effect of some inorganic anions. *Mater. Chem. Phys.* **2003**, 80, 696-703.

(14) Seruga, M. and Hasenay, D. Electrochemical and surface properties of aluminium in citric acid solutions. *J. Appl. Electrochem.* **2001**, 31, 961-967.

(15) Kristiansen, B., Mattey, M., and Linden, J. *Citric Acid and Biotechnology*. 1999, Philadelphia, PA: Taylor & Francis Inc.

(16) Krauskopf, K. *Introduction to Geochemistry*. 3rd ed. 1995, New York: McGraw-Hill.

(17) Morgan, J. J. Manganese in natural waters and earth's crust: Its availability to organisms. In *Metal Ions in Biological Systems*, H. Sigel, Editor. 2000, Dekker: New York. 1-34.

(18) Davison, W. Iron and manganese in lakes. *Earth-Sci. Rev.* **1993**, 34, 119-163.

(19) Tournassat, C., Charlet, L., Bosbach, D., and Manceau, A. Arsenic(III) oxidation by birnessite and precipitation of manganese(II) arsenate. *Environ. Sci. Technol.* **2002**, 36, 493-500.

(20) Eary, L. E. and Rai, D. Kinetics of chromium(III) oxidation to chromium(VI) by reaction with manganese-dioxide. *Environ. Sci. Technol.* **1987**, 21, 1187-1193.

(21) Stone, A. T. and Morgan, J. J. Reduction and dissolution of manganese (III) and manganese (IV) oxides by organics. 1. Reaction with hydroquinone. *Environ. Sci. Technol.* **1984**, 18, 450-456.

(22) Stone, A. T. and Morgan, J. J. Reduction and dissolution of manganese (III) and manganese (IV) oxides by organics: 2. Survey of the reactivity of organics. *Environ. Sci. Technol.* **1984**, 18, 617-624.

(23) Stone, A. T. Reductive dissolution of manganese(III/IV) oxides by substituted phenols. *Environ. Sci. Technol.* **1987**, 21, 979-988.

(24) Xyla, A. G., Sulzberger, B., Luther, G. W., Hering, J. G., Vancappellen, P., and Stumm, W. Reductive dissolution of manganese(III,IV) (hydr)oxides by oxalate - the effect of pH and light. *Langmuir* **1992**, 8, 95-103.

(25) McArdell, C. S., Stone, A. T., and Tian, J. Reaction of EDTA and related aminocarboxylate chelating agents with $Co^{III}OOH$ (heterogenite) and $Mn^{III}OOH$ (manganite). *Environ. Sci. Technol.* **1998**, 32, 2923-2930.

(26) Klewicki, J. K. and Morgan, J. J. Dissolution of β–MnOOH particles by ligands: Pyrophosphate, ethylenediaminetetraacetate, and citrate. *Geochim. Cosmochim. Acta* **1999**, 63, 3017-3024.

(27) Nowack, B. and Stone, A. T. Homogeneous and heterogeneous oxidation of nitrilotrismethylenephosphonic acid (NTMP) in the presence of manganese (II, III) and molecular oxygen. *J. Phys. Chem. B* **2002**, 106, 6227-6233.

(28) Filius, J. D., Hiemstra, T., and Van Riemsdijk, W. H. Adsorption of small weak organic acids on goethite: Modeling of mechanisms. *J. Colloid Interf. Sci.* **1997**, 195, 368-380.

(29) Cornell, R. M. and Schindler, P. W. Infrared study of the adsorption of hydroxycarboxylic acids on α-FeOOH and amorphous Fe (III)hydroxide. *Colloid Polym. Sci.* **1980**, 258, 1171-1175.

(30) Geelhoed, J. S., Hiemstra, T., and Van Riemsdijk, W. H. Competitive interaction between phosphate and citrate on goethite. *Environ. Sci. Technol.* **1998**, 32, 2119-2123.

(31) Lackovic, K., Johnson, B. B., Angove, M. J., and Wells, J. D. Modeling the adsorption of citric acid onto muloorina illite and related clay minerals. *J. Colloid Interf. Sci.* **2003**, 267, 49-59.

(32) Whitehead, C. F. *Speciation of Carboxylate-Containing Chelating Agent in The Presence of Iron (Hydr)oxide Minerals and Metal Ions*. Ph.D. dissertation, 2003, The Johns Hopkins University: Baltimore, MD.

(33) Zhang, Y., Kallay, N., and Matijevic, E. Interactions of metal hydrous oxides with chelating-agents .7. Hematite-oxalic acid and hematite-citric acid systems. *Langmuir* **1985**, 1, 201-206.

(34) Godtfredsen, K. L. and Stone, A. T. Solubilization of manganese dioxide-bound copper by naturally occurring organic compounds. *Environ. Sci. Technol.* **1994**, 28, 1450-1458.

(35) Kostka, J. E., Luther, G. W., and Nealson, K. H. Chemical and biological reduction of Mn(III)-pyrophosphate complexes - potential importance of dissolved Mn(III) as an environmental oxidant. *Geochim. Cosmochim. Acta* **1995**, 59, 885-894.

(36) Luo, J. A., Zhang, Q. H., and Suib, S. L. Mechanistic and kinetic studies of crystallization of birnessite. *Inorg. Chem.* **2000**, 39, 741-747.

(37) Silvester, E., Manceau, A., and Drits, V. A. Structure of synthetic monoclinic Na-rich birnessite and hexagonal birnessite .2. Results from chemical studies and exafs spectroscopy. *Am. Mineral.* **1997**, 82, 962-978.

(38) Post, J. E. Manganese oxide minerals: Crystal structures and economic and environmental significance. *P. Natl Acad. Sci. USA* **1999**, 96, 3447-3454.

(39) Wang, X. and Li, Y. D. Synthesis and formation mechanism of manganese dioxide nanowires/nanorods. *Chem.-Eur. J.* **2003**, 9, 300-306.

(40) Clesceri, L. S., Eaton, A. D., and Greenberg, A. E., eds. *Standard Methods for the Examination of Water and Wastewater*. 20th ed. 2000, American Public Health Association; American Water Works Association; Water Pollution Control Federation: Washington, DC.

(41) Carbonaro, R. F. and Stone, A. T. Speciation of chromium(III) and cobalt(III) (amino)carboxylate complexes using capillary electrophoresis. *Anal. Chem.* **2005**, 77, 155-164.

(42) Burgisser, C. S. and Stone, A. T. Determination of EDTA, NTA, and other amino carboxylic acids and their Co(II) and Co(III) complexes by capillary electrophoresis. *Environ. Sci. Technol.* **1997**, 31, 2656-2664.

(43) Cotton, F. A., Wilkinson, G., Murillo, C. A., and Bochmann, M. *Advanced Inorganic Chemistry*. 6th ed. 1999, New York: Wiley Interscience. 757-775.

(44) Shriver, D., and Atkins, P. *Inorganic Chemistry*. 3rd ed. 1999, New York: W.H. Freeman and Company.

(45) Press, W. H., Flannery, B. P., Teukolsky, S. A., and Vetterling, W. T. *Numerical Recipes*. 1986, Cambridge: Cambridge University Press.

(46) Datta, S. P., Grzybows.Ak, and Tate, S. S. Metal-catalysed decomposition of α-hydroxypolycarboxylic acids. *Nature* **1965**, 207, 1047-1049.

(47) Khan, Z., Akram, M., and Kabir Ud, D. A kinetic study of the one-step three-electron oxidation of citric acid by chromium(VI). *Oxid. Commun.* **2001**, 24, 257-267.

(48) Larson, R. A. and Rockwell, A. L. Chloroform and chlorophenol production by decarboxylation of natural acids during aqueous chlorination. *Environ. Sci. Technol.* **1979**, 13, 325-329.

(49) Abrahamson, H. B., Rezvani, A. B., and Brushmiller, J. G. Photochemical and spectroscopic studies of complexes of iron(III) with citric acid and other carboxylicacids. *Inorg. Chim. Acta* **1994**, 226, 117-127.

(50) Stone, A. T., Godtfredsen, K. L., and Deng, B. L. Sources and reactivity of reductants encountered in aquatic environments. In *Chemistry of Aquatic Systems: Local and Global Perspectives*, G. Bidoglio and W. Stumm, Editors. 1994, Kluwer: Dordrecht, the Netherlands. 337-374.

(51) Houghton, R. P. *Metal Complexes in Organic Chemistry*. Cambridge texts in chemistry and biochemistry, ed. D.T. Elmore, et al. 1979, London: Cambridge University Press.

(52) Stone, A. T. and Morgan, J. J. Chapter 9: Reductive dissolution of metal oxides. In *Aquatic surface chemistry: Chemical Processes at the Particle-Water Interface*, W. Stumm, Editor. 1987, John Wiley: New York. 221-254.

(53) Logan, S. R. *Fundamentals of Chemical Kinetics*. 1996, Essex, England: Longman Group Limited.

(54) Epstein, I. R. and Pojman, J. A. *An Introduction to Nonlinear Chemical Dynamics: Oscillations, Waves, Patterns, and Chaos*. 1998, New York: Oxford University Press.

(55) Bazsa, G., Nagy, I. P., and Lengyel, I. The nitric-acid nitrous-acid and ferroin ferriin system - a reaction that demonstrates autocatalysis, reversibility, pseudo orders, chemical waves, and concentration jump. *J. Chem. Educ.* **1991**, 68, 863-868.

(56) Kurin-Csorgei, K., Epstein, I. R., and Orban, M. New heterogeneous chemical oscillators: Reduction of manganese species by hypophosphite on a Pt surface. *J. Phys. Chem. B* **2004**, 108, 7352-7358.

(57) Martell, A. E., Smith, R. M., and Motekaitis, R. J. *NIST Critically Selected Stability Constants of Metal Complexes Database*. 2004, US Department of Commerce, National Institute of Standards and Technology: Gaithersburg, MD.

(58) Carberry, J. J. *Chemical and Catalytic Reaction Engineering*. 1976, New York: McGraw-Hill.

(59) Fogler, S. *Elements of Chemical Reaction Engineering*. 2nd ed. 1992, Englewood Cliffs, NJ: Prentice Hall.

(60) Yao, W. S. and Millero, F. J. Adsorption of phosphate on manganese dioxide in seawater. *Environ. Sci. Technol.* **1996**, 30, 536-541.

(61) Cambier, P. and Sposito, G. Adsorption of citric-acid by synthetic pseudoboehmite. *Clay Clay Miner.* **1991**, 39, 369-374.

(62) Kummert, R. and Stumm, W. The surface complexation of organic-acids on hydrous γ-Al_2O_3. *J. Colloid Interf. Sci.* **1980**, 75, 373-385.

(63) Jardine, P. M. and Taylor, D. L. Kinetics and mechanisms of Co(II)EDTA oxidation by pyrolusite. *Geochim. Cosmochim. Acta* **1995**, 59, 4193-4203.

(64) Carbonaro, R. F. *Sources, Sinks, and Speciation of Chromium(III) (Amino)carboxylate Complexes in Heterogeneous Aqueous Media*, in *Department of Geography and Environmental Engineering*. Ph.D. dissertation, 2004, The Johns Hopkins University: Baltimore. Chapter 3.

(65) Baumgartner, E., Blesa, M. A., Marinovich, H. A., and Maroto, A. J. G. Heterogeneous electron-transfer as a pathway in the dissolution of magnetite in oxalic-acid solutions. *Inorg. Chem.* **1983**, 22, 2224-2226.

(66) Blesa, M. A., Marinovich, H. A., Baumgartner, E. C., and Maroto, A. J. G. Mechanism of dissolution of magnetite by oxalic acid-ferrous ion solutions. *Inorg. Chem.* **1987**, 26, 3713-3717.

(67) Afonso, M. D., Morando, P. J., Blesa, M. A., Banwart, S., and Stumm, W. The reductive dissolution of iron-oxides by ascorbate - the role of carboxylate anions in accelerating reductive dissolution. *J. Colloid Interf. Sci.* **1990**, 138, 74-82.

(68) Suter, D., Banwart, S., and Stumm, W. Dissolution of hydrous iron(III) oxides by reductive mechanisms. *Langmuir* **1991**, 7, 809-813.

(69) Ballesteros, M. C., Rueda, E. H., and Blesa, M. A. The influence of iron (II) and (III) on the kinetics of goethite dissolution by EDTA. *J. Colloid Interf. Sci.* **1998**, 201, 13-19.

(70) Sulzberger, B., Suter, D., Siffert, C., Banwart, S., and Stumm, W. Dissolution of Fe(III)(hydr)oxides in natural-waters - laboratory assessment on the kinetics controlled by surface coordination. *Mar. Chem.* **1989**, 28, 127-144.

(71) Klewicki, J. K. and Morgan, J. J. Kinetic behavior of Mn(III) complexes of pyrophosphate, EDTA, and citrate. *Environ. Sci. Technol.* **1998**, 32, 2916-2922.

(72) Laha, S. and Luthy, R. G. Oxidation of aniline and other primary aromatic-amines by manganese-dioxide. *Environ. Sci. Technol.* **1990**, 24, 363-373.

Table 2.1. Effect of Additives on Rates of 3-Ketoglutarate Production (r_{max}) for 200 mM MnO_2 Suspensions Containing 200 mM Citrate, and 10 mM MOPS buffer (pH 7.1).

Additive	r_{max} (μM/h)	Normalized rate
-	13.6	1.0
10 μM Zn^{II}	11.8	0.87
200 μM Zn^{II}	0.9	0.066
10 μM Mn^{II}	13.7	1.0
200 μM Mn^{II}	11.3	0.83
500 μM Mn^{II}	6.6	0.49
1000 μM Mn^{II}	4.0	0.29

Table 2.2. Mn^{II} Aqueous Phase Speciation Calculations in Support of Additive Experiments. Conditions: 10 mM Mn^{II}, 200 mM Citrate, pH 7.1, 10 mM Ionic Strength. (Citrate Ligand is Abbreviated as Cit.)

No Additive	10 μM Zn^{II}	200 μM Zn^{II}
8.46 μM $Mn^{II}cit^{-}$	8.48 μM $Mn^{II}cit^{-}$	3.59 μM $Mn^{II}cit^{-}$
1.51 μM Mn^{2+}	1.50 μM Mn^{2+}	6.39 μM Mn^{2+}
0.022 μM $Mn^{II}Hcit^{0}$	0.022 μM $Mn^{II}Hcit^{0}$	0.0092 μM $Mn^{II}Hcit^{0}$
5.0 mM Orthophosphate	0.20 mM Pyrophosphate (PP)	
5.78 μM $Mn^{II}cit^{-}$	6.21 μM $Mn^{II}cit^{-}$	
1.02 μM Mn^{2+}	1.09 μM Mn^{2+}	
0.015 μM $Mn^{II}Hcit^{0}$	0.016 μM $Mn^{II}Hcit^{0}$	
3.18 μM $Mn^{II}HPO_4^{0}$	2.68 μM $Mn^{II}PP^{2-}$	

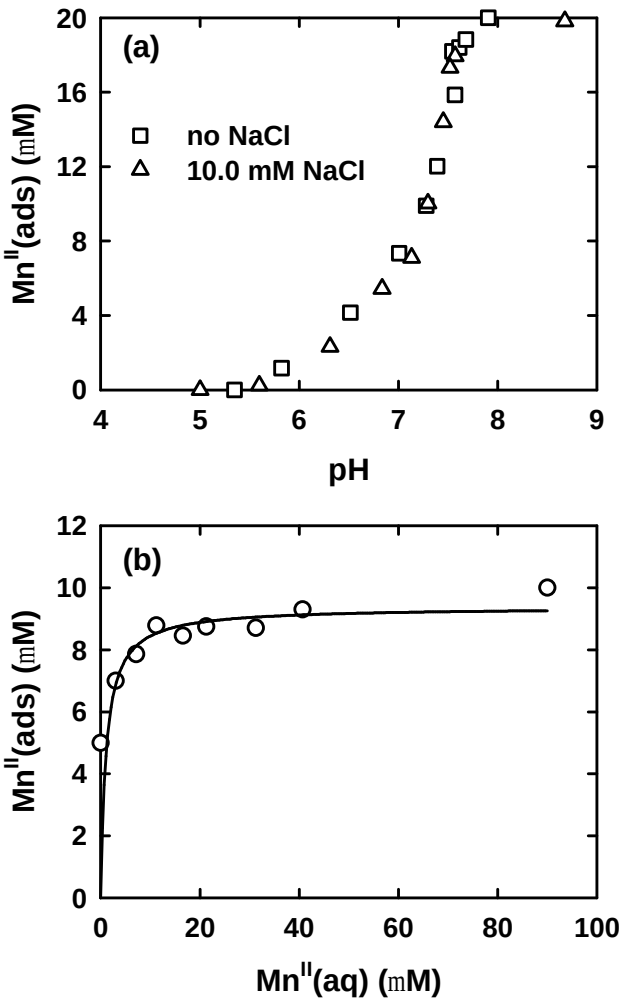

Figure 2.1. Mn^{II} adsorption onto 200 mM MnO_2 as a function of (a) pH and (b) [Mn^{II}(aq)]. In (a), 20 mM Mn^{II} was employed, and the pH was fixed using HCl and NaOH additions. In (b), the pH was set using 10 mM MOPS buffer (pH 7.1); the fitted line corresponds to a fit to the Langmuir Equation (see text).

(a) From citrate to 3-ketoglutarate: oxidative decarboxylation

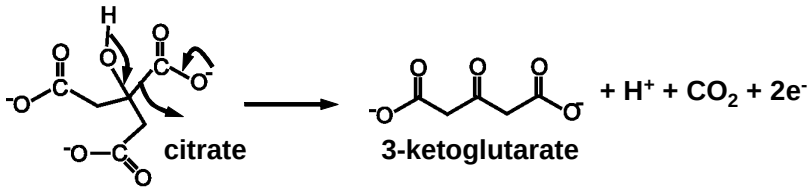

(b) From 3-ketoglutarate to acetoacetate: nonredox decarboxylation

Case 1: decarboxylation without metal ion participation

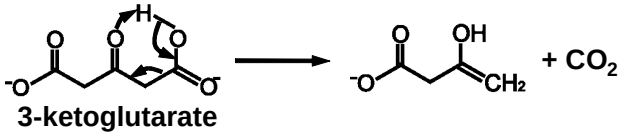

Case 2: metal ion-catalyzed decarboxylation

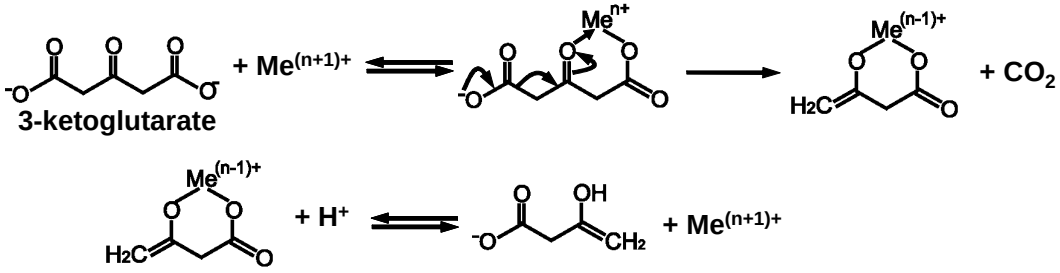

rapid tautomerization:

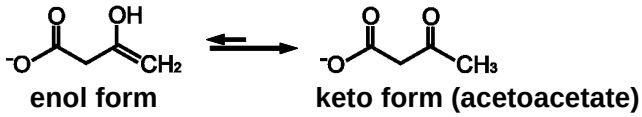

Figure 2.2. Mechanisms for (a) the oxidative decarboxylation of citrate, yielding 3-ketoglutarate, and (b) the non-redox rearrangement of 3-ketoglutarate, yielding acetoacetate *(51)*.

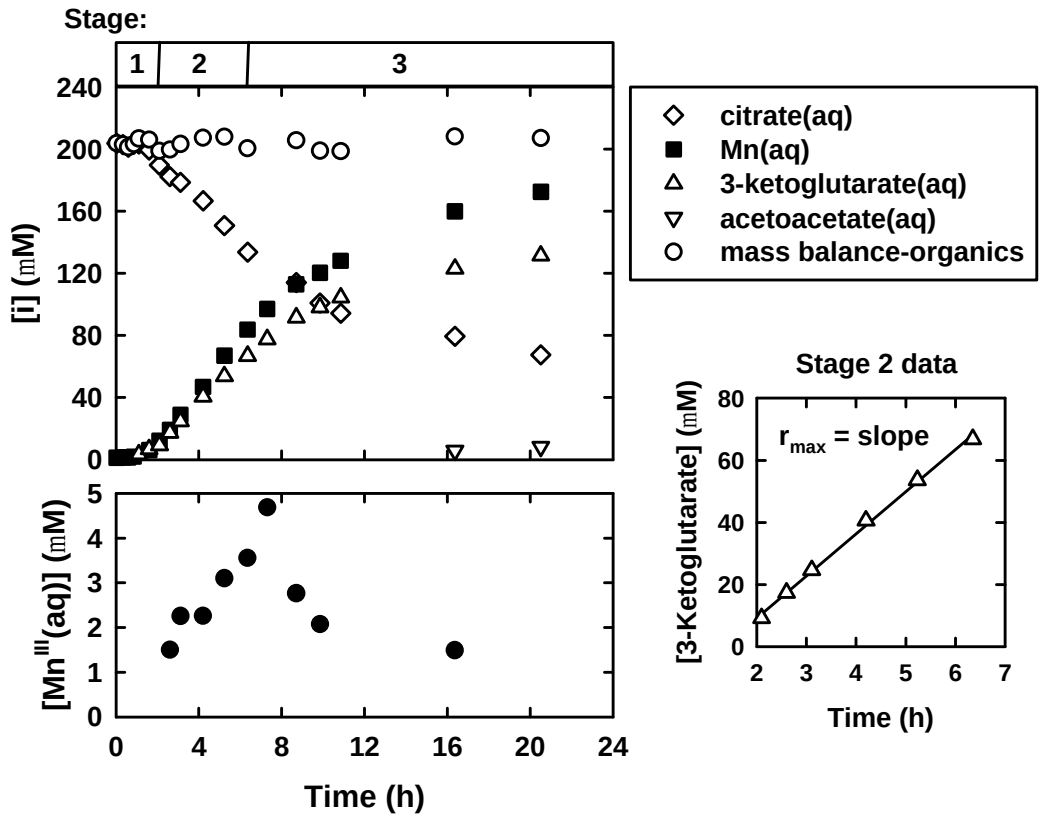

Figure 2.3. Illustrative time course for the reaction of 200 mM citrate with 200 mM MnO_2 in suspensions containing 10 mM MOPS buffer (pH 7.1) and 10 mM NaCl. The mass balance refers to the sum [citrate(aq)] + [3-ketoglutarate(aq)] + [acetoacetate(aq)]. An initial induction period (Stage 1) is followed by an acceleratory stage (Stage 2) and eventual deceleration (Stage 3) as reactants become depleted.

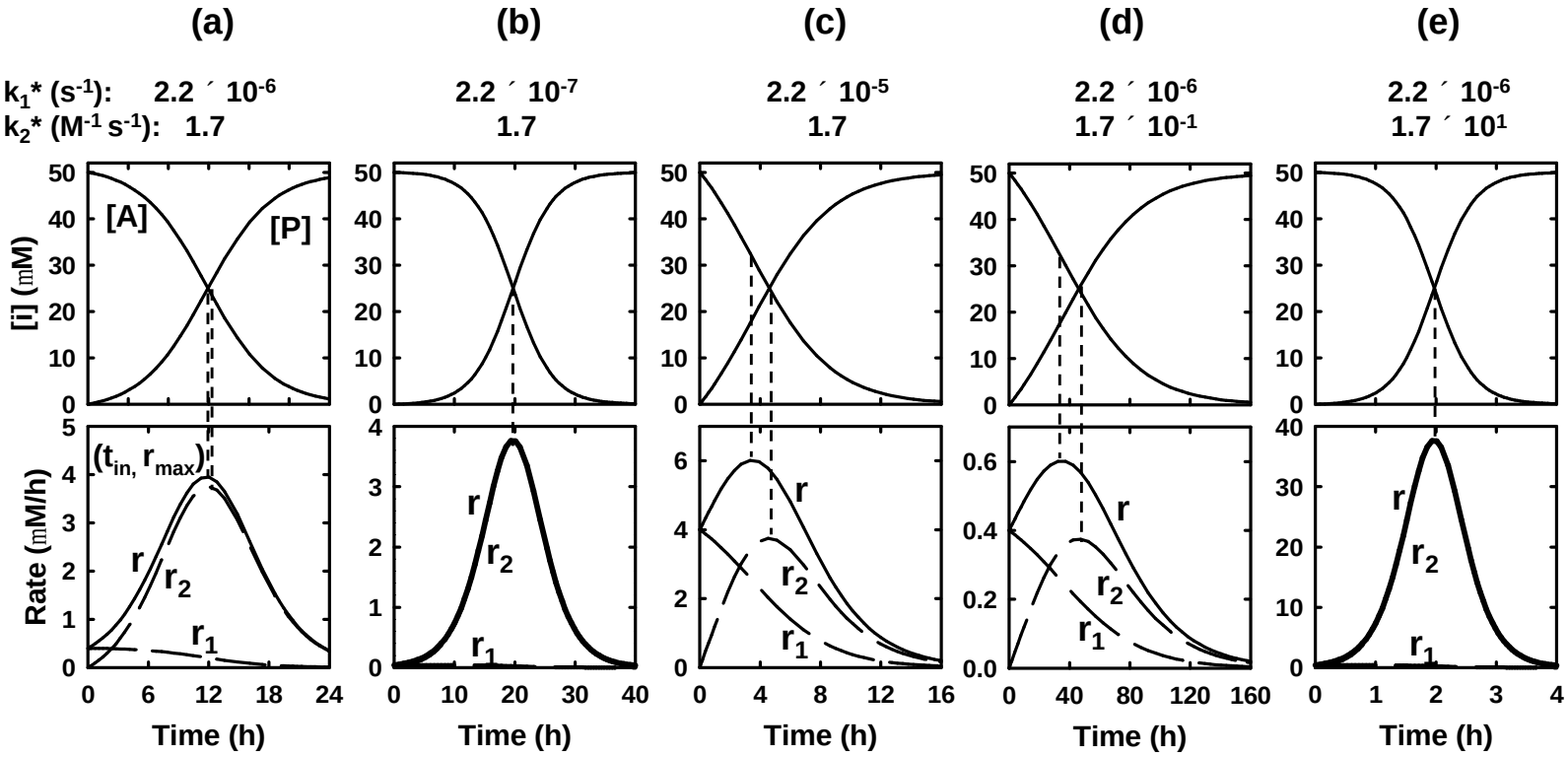

Figure 2.4. Simulated time course plots (upper) and rates as a function of time (lower, corresponding to the first derivative) based upon Reactions 1 and 2 presented in the text. (a) represents the best fit to an experiment employing $[Citrate]_o$ = 50 mM and $[MnO_2]_o$ = 200 mM, pH 7.1.

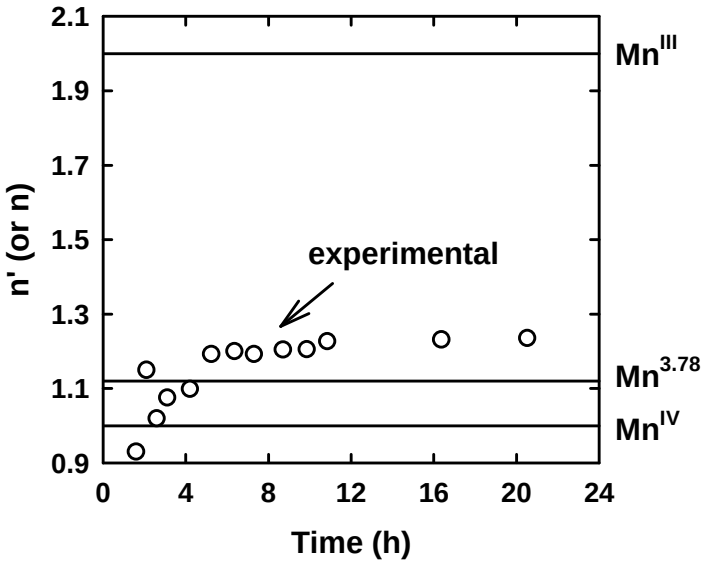

Figure 2.5. Yield of Mn^{II} per mole of citrate oxidized (see text) for a suspension containing 200 mM citrate, 200 mM MnO_2, and 10 mM MOPS buffer (pH 7.1). Experimental values (n') were obtained from the experiment presented in Figure 2.3. Theoretical values (n) are shown as straight lines for a (hydr)oxide consisting solely of Mn^{III}, for one consisting solely of Mn^{IV}, and for one where the average manganese oxidation state is +3.78.

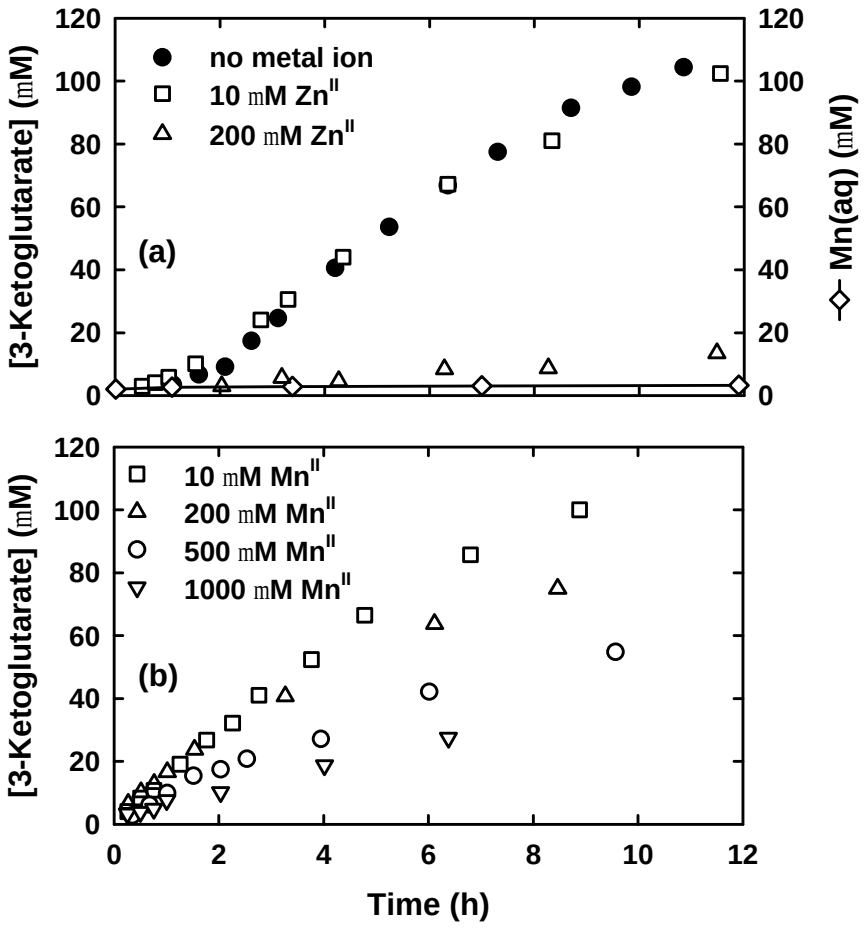

Figure 2.6. The effect of adding (a) Zn^{II} and (b) Mn^{II} at the onset of the reaction. In the upper plot, the symbol -à- corresponds to Mn(aq) released when 200 mM Zn^{II} is added without citrate. Reaction conditions: 200 mM citrate, 200 mM MnO_2, and 10 mM MOPS buffer (pH 7.1).

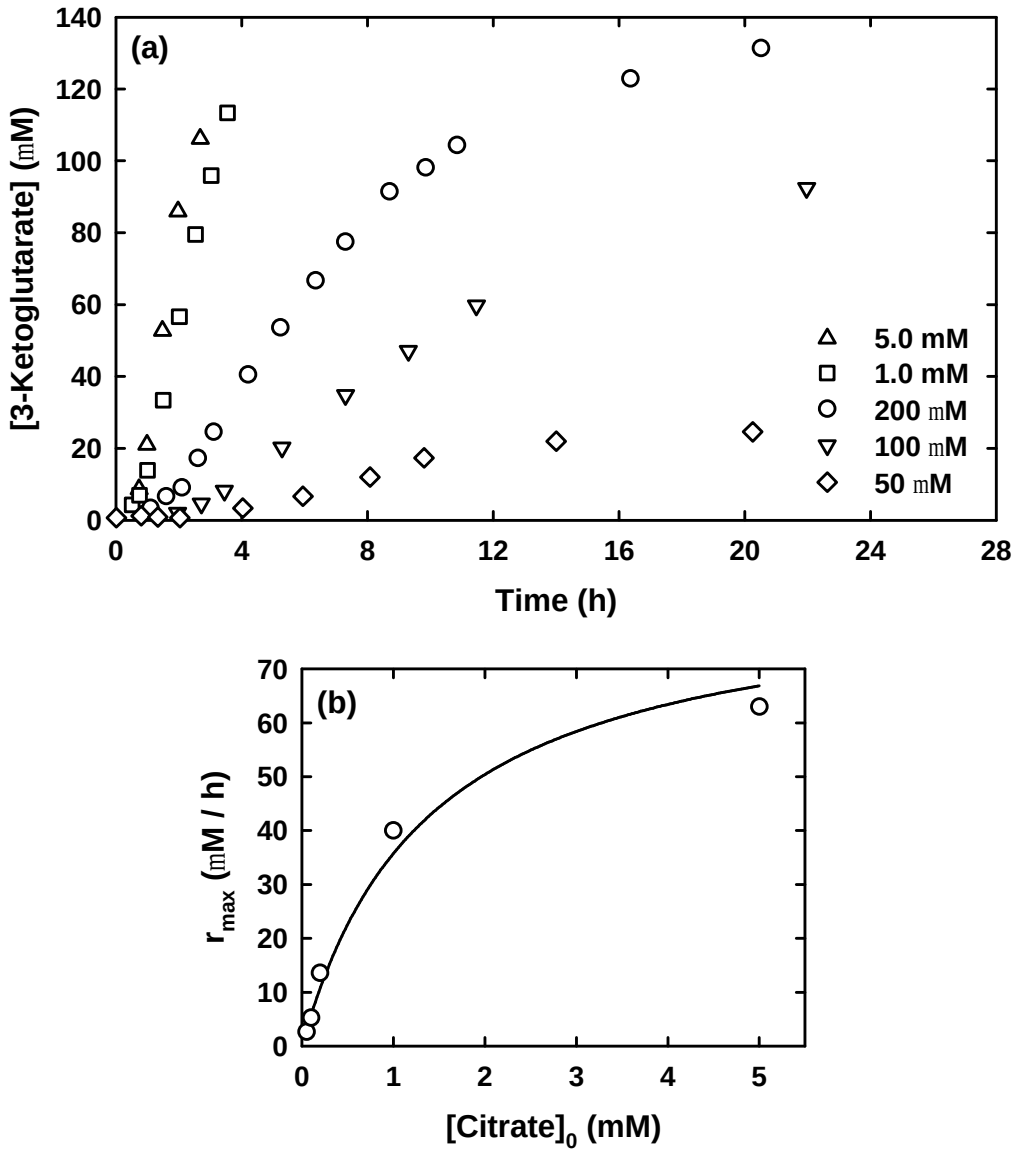

Figure 2.7. Effect of increasing citrate concentration on (a) 3-ketoglutarate production; (b) r_{max}, the fitted line corresponds to a fit to the Langmuir-Hinshelwood rate expression (see text). All suspensions contained 200 mM MnO_2 and 10 mM MOPS (pH 7.1).

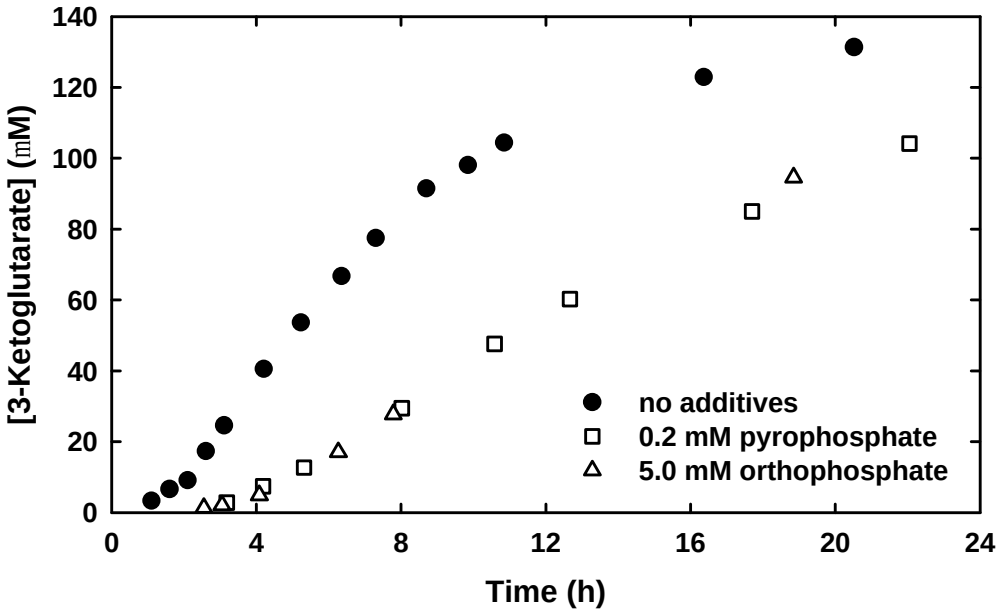

Figure 2.8. Effects of adding pyrophosphate and orthophosphate at the onset of reaction. Reaction conditions: 200 mM citrate, 200 mM MnO_2, and 10 mM MOPS buffer (pH 7.1).

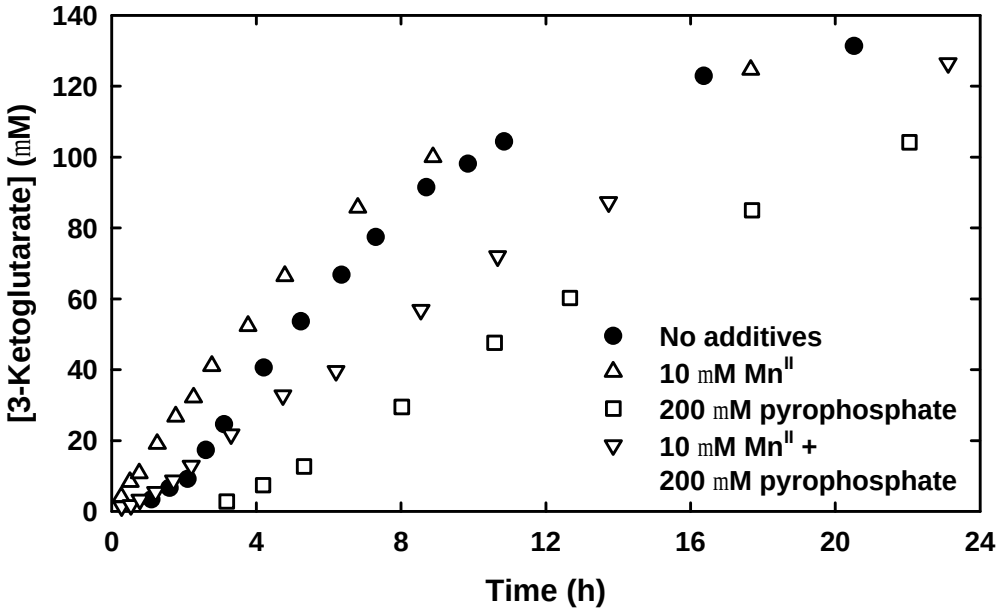

Figure 2.9. Effects of adding Mn^{II} and pyrophosphate, alone or together, at the onset of reaction. Reaction conditions: 200 mM citrate, 200 mM MnO_2, and 10 mM MOPS buffer (pH 7.1).

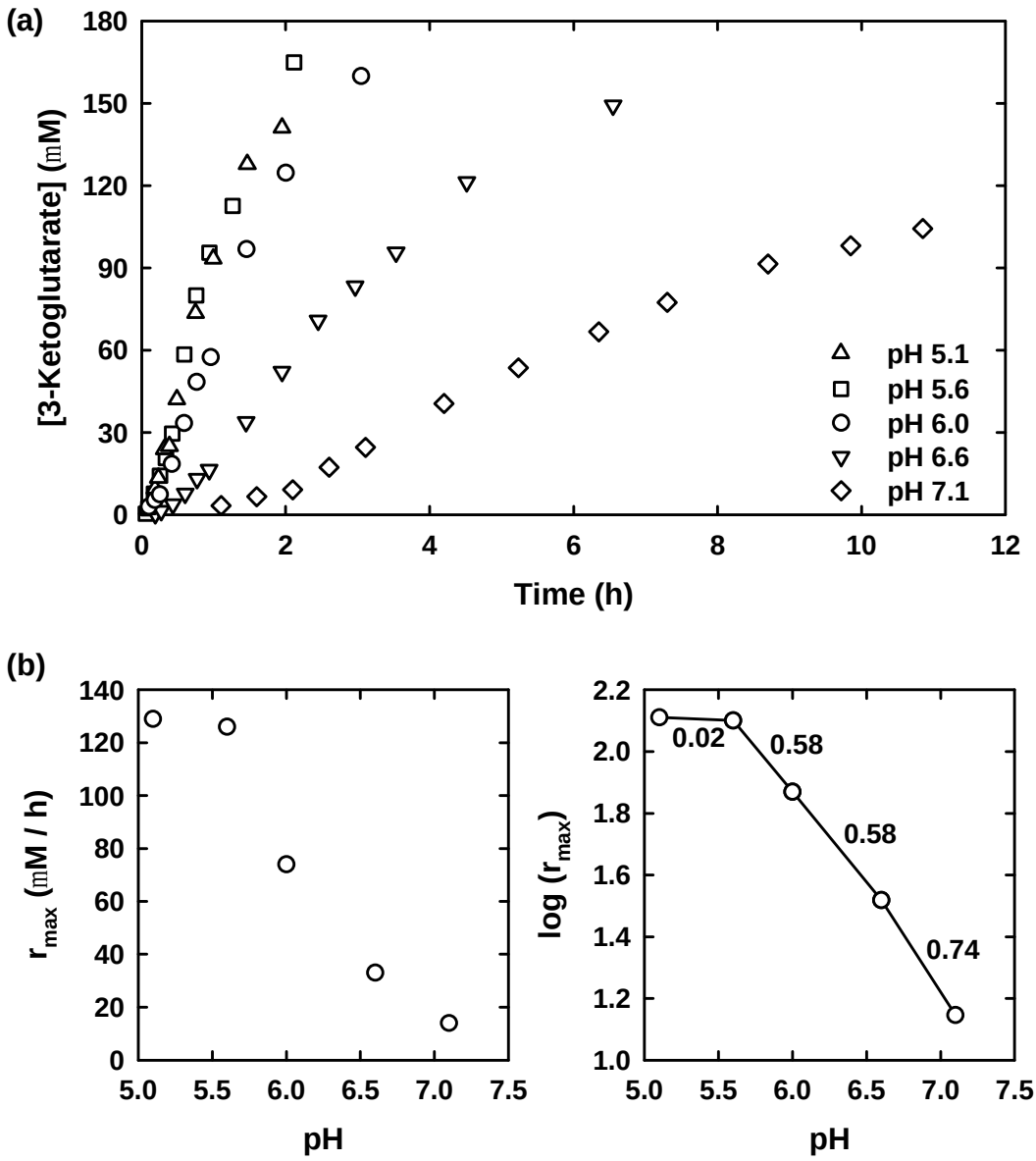

Figure 2.10. (a) Time course plots for 3-ketoglutarate production as a function of pH. (b) r_{max} as a function of pH (semi-log plot is shown on the left. The log-log plot on the right shows the order with respect to $[H^+]$ as the slope for lines connecting successive pairs of points.) All suspensions contained 200 mM MnO_2, and 10 mM pH buffer. (Butyrate buffer was used for pH 5.1 and 5.6; MES for pH 6.0 and 6.6; MOPS for pH 7.1.)

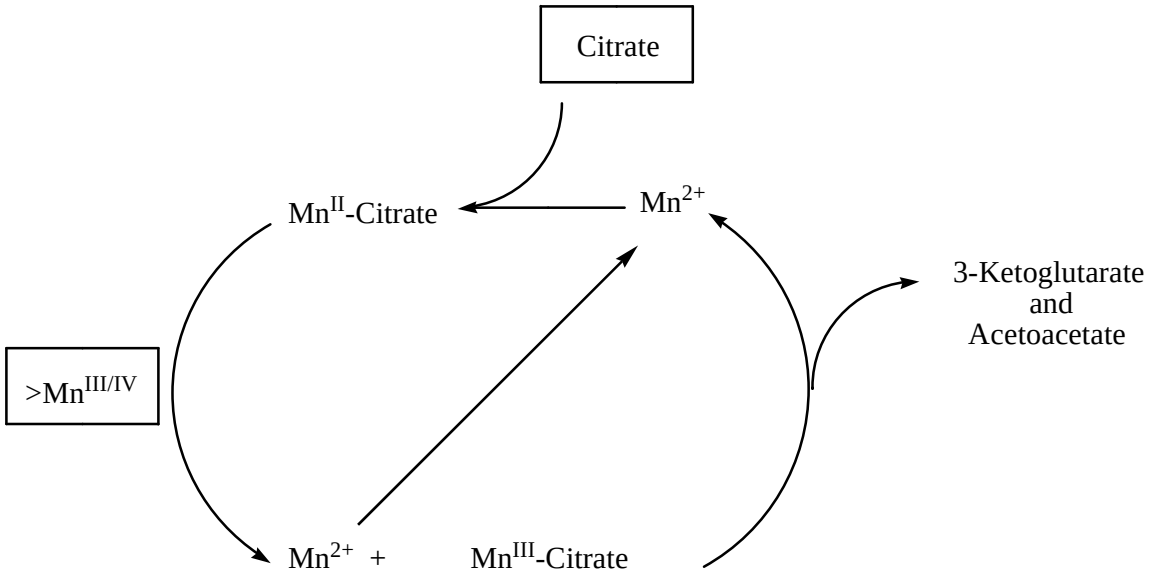

Figure 2.11. Interfacial $Mn^{III/II}$ citrate reactions responsible for autocatalysis.